THE JOURNAL OF BIOLOGICAL CHEMISTRY VOL. 291, NO. 12, pp. 6376–6385, March 18, 2016

Structural Basis for Nucleotide Hydrolysis by the Acid Sphingomyelinase-like Phosphodiesterase SMPDL3A*

Received for publication, December 17, 2015, and in revised form, January 15, 2016 Published, JBC Papers in Press, January 20, 2016, DOI 10.1074/jbc.M115.711085

Alexei Gorelik[‡1], **Katalin Illes**[‡], **Giulio Superti-Furga**[§], **and Bhushan Nagar**[‡2]

From the [‡]*Department of Biochemistry and Groupe de Recherche Axe sur la Structure des Proteines, Faculty of Medicine, McGill University, Montreal, Quebec H3G 0B1, Canada and* [§]*CeMM Research Center for Molecular Medicine of the Austrian Academy of Sciences, A-1090 Vienna, Austria*

Sphingomyelin phosphodiesterase, acid-like 3A (SMPDL3A) is a member of a small family of proteins founded by the well characterized lysosomal enzyme, acid sphingomyelinase (ASMase). ASMase converts sphingomyelin into the signaling lipid, ceramide. It was recently discovered that, in contrast to ASMase, SMPDL3A is inactive against sphingomyelin and, surprisingly, can instead hydrolyze nucleoside diphosphates and triphosphates, which may play a role in purinergic signaling. As none of the ASMase-like proteins has been structurally characterized to date, the molecular basis for their substrate preferences is unknown. Here we report crystal structures of murine SMPDL3A, which represent the first structures of an ASMase-like protein. The catalytic domain consists of a central mixed β-sandwich surrounded by α-helices. Additionally, SMPDL3A possesses a unique C-terminal domain formed from a cluster of four α-helices that appears to distinguish this protein family from other phosphoesterases. We show that SMDPL3A is a di-zinc-dependent enzyme with an active site configuration that suggests a mechanism of phosphodiester hydrolysis by a metal-activated water molecule and protonation of the leaving group by a histidine residue. Co-crystal structures of SMPDL3A with AMP and α,β-methylene ADP (AMPCP) reveal that the substrate binding site accommodates nucleotides by establishing interactions with their base, sugar, and phosphate moieties, with the latter the major contributor to binding affinity. Our study provides the structural basis for SMPDL3A substrate specificity and sheds new light on the function of ASMase-like proteins.

Sphingomyelin is a major lipid constituent of mammalian cellular membranes. Hydrolysis of sphingomyelin (SM)[3] to ceramide and phosphocholine by sphingomyelinase enzymes (SMases) alters membrane properties and can result in the formation of signaling platforms, thus facilitating signal transduction (1). Mammalian SMases are classified into three categories based on their pH optimum (2). The lone alkaline SMase metabolizes SM in the intestinal tract (3), whereas neutral SMases are active on the cytosolic side of the plasma membrane and in various organelles (4). The acid sphingomyelinase (ASMase) is found mainly in lysosomes; however, a fraction of this protein is secreted where it can act on the extracellular side of the plasma membrane and on lipoproteins in the circulation (5).

ASMase is a member of a small family of three paralogs that also includes SMPDL3A and SMPLD3B. The latter two proteins are poorly characterized compared with ASMase. SMPDL3B was recently shown to be a negative regulator of the immune signaling response induced by Toll-like receptors, and deficiency of this enzyme changes the cellular lipid composition and membrane fluidity (6). Given its role in membrane modulation and the fact that SMPDL3B is anchored to the membrane via a glycosylphosphatidylinositol link (7), its substrate is likely to be a membrane constituent like SM. The substrate and function of SMPDL3A, however, are less clear. This enzyme is secreted by osteoclasts (8), adipocytes (9), astrocytes (10), and macrophages (11), where it is up-regulated by the activation of the liver X receptor (12, 13). In the serum, SMPDL3A interacts with apolipoprotein A1 (14, 15). Its expression is increased in the vasculature in obesity (16), in atherosclerotic lesions (17), and in drug-induced phospholipidosis (18, 19). These findings suggested a lipid-related role for SMPDL3A in the circulation. Additionally, the mannose 6-phosphate lysosomal targeting signal has been detected on this protein from multiple tissues (20), showing that SMPDL3A is transported to lysosomes (21). However, its lysosomal targeting is reduced during pathological accumulation of cholesterol and glycolipids in that compartment (22).

More recently, SMPDL3A was reported to be a phosphoesterase up-regulated by cholesterol in macrophages (11). Surprisingly, the enzyme was found to be inactive against SM

* This work is based upon research conducted at the Cornell High Energy Synchrotron Source (CHESS), which is supported by the National Science Foundation and the NIGMS, National Institutes of Health under National Science Foundation Grant DMR-1332208 using the Macromolecular Diffraction at CHESS (MacCHESS) facility, which is supported by National Institutes of Health Grant GM-103485 (NIGMS). The authors declare that they have no conflicts of interest with the contents of this article. The content is solely the responsibility of the authors and does not necessarily represent the official views of the National Institutes of Health.

The atomic coordinates and structure factors (codes 5FC1, 5FC5, 5FC6, 5FC7, 5FCA, and 5FCB) have been deposited in the Protein Data Bank (http://wwpdb.org/).

[1] Supported by a graduate scholarship from the CREATE Training Program in Bionanomachines.

[2] Supported by a Canada Research Chair and an operating grant from the Canadian Institutes of Health Research (CIHR Grant MOP-133535). To whom correspondence should be addressed: Rm. 464, 3649 promenade Sir-William-Osler, Montreal, Quebec H3G 0B1, Canada. Tel.: 514-398-7272; Fax: 514-398-2983; E-mail: bhushan.nagar@mcgill.ca.

[3] The abbreviations used are: SM, sphingomyelin; SMPDL3A, sphingomyelin phosphodiesterase, acid-like 3A; SMase, sphingomyelinase; ASMase, acid sphingomyelinase; AMPCP, α,β-methylene ADP; AMPCPP, α,β-methylene ATP; CTD, C-terminal domain.

or other lipids but instead active in the hydrolysis of nucleotide diphosphates and triphosphates (11). An anti-inflammatory role as a moderator of nucleotide-based purinergic signaling was, therefore, proposed for this protein. Furthermore, SMPDL3A was shown to be inhibited by zinc, whereas its close homolog, ASMase, is a zinc-dependent enzyme (5). A recently discovered bacterial ASMase-like protein, RsASML, also displayed no activity against SM but was able to hydrolyze ATP and ADP (23). This bacterial enzyme shares 23% sequence identity with human SMPDL3A, which is in turn 39% identical to SMPDL3B and 29% identical to ASMase.

These reports revealed an unexpected divergence of substrate specificity within the ASMase-like family. As neither ASMase nor its paralogs has been structurally characterized, the basis for their substrate preferences remains unknown. Here we present high resolution crystal structures of murine SMPDL3A bound to several small molecules. The protein adopts a β-sandwich fold surrounded by α-helices and has a unique C-terminal domain. Structures of the enzyme bound to AMP and an ADP analog explain its ability to accommodate nucleotide substrates and its lack of activity against SM. Based on the active site arrangement and enzymatic assay results, a catalytic mechanism for the hydrolysis of nucleotides is proposed.

Experimental Procedures

Constructs—SMPDL3A from mouse (residues 23–445; Uniprot #P70158) and human (residues 23–453; Uniprot # Q92484) were subcloned into a derivative of pFastBac 1 (Invitrogen). The vector contained the melittin signal peptide MKFLVNVALVFMVVYISYIYA followed by a hexahistidine tag DRHHHHHHKL.

Protein Expression and Purification—Recombinant baculoviruses were generated according to the Bac-to-Bac Baculovirus Expression System protocol (Invitrogen) with minor modifications; DH10MultiBac cells were used (24), and viruses were added to *Sf*9 cells grown in I-Max medium (Wisent Bioproducts). Protein expression took place at 27 °C for 64 h. Subsequent steps were carried out at 4 °C. Cells were removed by centrifugation at 1000 × *g* then at 9000 × *g*, and supernatants containing the secreted protein were incubated with HisPur nickel-nitrilotriacetic acid resin (Thermo Fisher Scientific). The beads were washed with buffer A (50 mM Tris-HCl, pH 7.5, 500 mM NaCl, 1 mM $MgCl_2$) and eluted with buffer A containing 250 mM imidazole. Proteins were concentrated and loaded on a Superdex 200 10/300 GL size-exclusion column (GE Healthcare) equilibrated with buffer B (15 mM Tris-HCl, pH 7.5, 100 mM NaCl). Proteins were concentrated to 10 mg ml^{-1} and flash-frozen.

Enzymatic Assay with Generic Phosphodiesterase Substrate—Protein at 50 nM was incubated with 1.7 mM bis(*p*-nitrophenyl) phosphate in assay buffer (100 mM NaCl and 100 mM Tris-HCl, pH 7.5, or sodium acetate, pH 5) at 37 °C. 100 mM NaOH was then added before measuring absorbance at 405 nm. The change in absorbance after 30 min was used for obtaining the normalized activity rates.

Enzymatic Assay with Nucleotide Substrate—The Biomol Green phosphate detection method (Enzo Life Sciences) was slightly modified. Protein at 1 nM to 2 μM was incubated with 4.35 μM to 2 mM ATP in assay buffer supplemented with 5 μM $ZnCl_2$ at 37 °C. Four volumes of Biomol Green reagent were added followed by incubation and absorbance measurement at 620 nm. The difference in absorbance after 15 min of ATP hydrolysis by SMPDL3A was used to interpolate the amount of phosphate produced via a standard curve. Linearity of the initial rates was ensured by comparing the result with those of a 30-min hydrolysis reaction. Michaelis-Menten parameters were obtained by nonlinear regression of the initial rates at varying ATP concentrations.

Crystallization and Data Collection—Crystals were grown by hanging drop vapor diffusion at 22 °C. Protein at 10 mg ml^{-1} in buffer B was mixed with an equal volume of well solution. Murine SMPDL3A was crystallized in 0.2 M $(NH_4)_2SO_4$, 0.1 M sodium acetate, pH 4.6, and 25% PEG 4000. For anomalous diffraction experiments, crystals were soaked in well solution supplemented with 20 mM $ZnCl_2$. Ligand-bound structures were obtained by crystallizing the protein in the presence of 50 mM phosphocholine, AMP, or α,β-methylene ATP (AMPCPP). All crystals were briefly soaked in well solution supplemented with 20% glycerol before flash-freezing. Diffraction data were collected at 100 K on beamlines 08ID-1 and 08B1-1 at the Canadian Macromolecular Crystallography Facility, Canadian Light Source, and on beamline MacCHESS F1, Cornell High Energy Synchrotron Source. Data were processed with HKL2000 (25).

Structure Determination and Refinement—The structure of murine SMPDL3A was solved by zinc single-wavelength anomalous diffraction using Autosol in Phenix (26) and manually rebuilt in Coot (27). Subsequent structures were obtained by molecular replacement using Phaser in Phenix. Refinement was performed with phenix.refine. Data processing and refinement statistics are presented in Table 1.

Results

Overall Structure of SMPDL3A—We determined the crystal structure of full-length murine SMPDL3A, which shares 80% identity with human SMPDL3A (Fig. 1). Our construct excluded the N-terminal signal peptide, which is normally not present in the mature protein, and extends from residues 23 to 445. The structure was solved at 1.8 Å resolution using SAD phasing from two tightly bound zinc ions in the active site. All subsequent structures with ligands were solved with molecular replacement (see Table 1 for data collection and refinement statistics). The enzyme adopts a relatively spherical shape with overall dimensions of 42 Å × 46 Å × 48 Å (Fig. 2*A*). The structure consists of two mixed β-sheets at its core flanked by α-helices (Fig. 2*B*); this architecture classifies it as a member of the calcineurin-like phosphoesterase structural superfamily (PFAM code PF00149, Fig. 2*C*), which also contains nucleotidases and, most notably, the PPP family of serine/threonine phosphatases (28). Both β-sheets contain six strands and form a mixed β-sandwich closed at one end and open at the other. The closed end as well as both longitudinal sides of the sandwich are surrounded by a total of seven α-helices. In addition, the structure includes a helical C-terminal domain (CTD). The CTD forms a cluster of four α-helices packed up against the open end

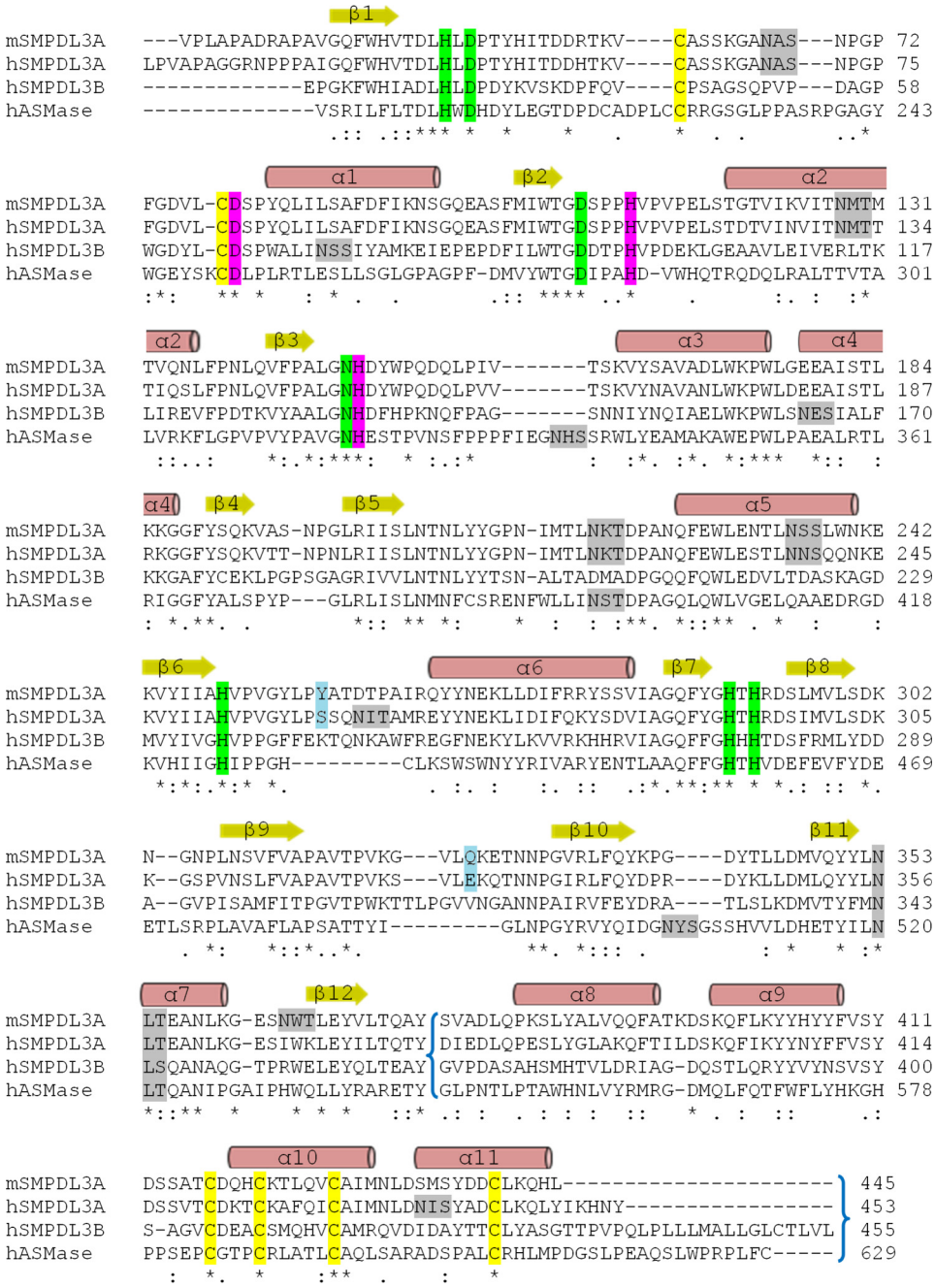

FIGURE 1. **Sequence alignment of SMPDL3A and ASMase.** The amino acid sequences of the catalytic and C-terminal domains (CTD) of human (*h*-) and murine (*m*-) SMPDL3A (80% identity) as well as of human ASMase (29% identity to SMPDL3A) and SMPDL3B (39% identity) are aligned. Cysteines involved in conserved disulfide bonds are highlighted in *yellow*, metal-coordinating residues are in *green*, and potential *N*-glycosylation sites are in *gray*. The two histidines and the aspartic acid involved in phosphate binding or catalysis are colored in *pink*. The tyrosine and the glutamine forming the sides of a cleft, which accommodates the adenine base of nucleotides, are shown in *blue*, as are the corresponding residues of human SMPDL3A. The CTD is delimited by *blue brackets*. Secondary structure elements of murine SMPDL3A are shown as *red cylinders* for helices and *yellow arrows* for strands.

of the β-sandwich, burying ~1900 Å^2 of surface area, and is unique to the three ASMase-like proteins in mammals (Fig. 1). The interface between the domains is formed mainly by hydrophobic contacts as well as multiple hydrogen bonds. Two disulfide bonds stabilize the CTD, and another disulfide bridge is present in the catalytic domain. The structure is also decorated by six *N*-linked glycans. Human SMPDL3A (11) shares five of these glycosylation sites and has two additional potential sites that correspond to surface-exposed locations in the structure.

Active Site Configuration—The active site of SMPDL3A is in a depression on the surface of the protein formed by loops extending from the central β-sheets. At its core are found two metal ions coordinated by the side chains of seven conserved residues (Fig. 3). A sulfate ion from the crystallization solution is positioned above the metals and coordinates them with two of its oxygen atoms. The third sulfate oxygen forms hydrogen bonds with two nearby histidines, His-149 and His-111. An additional interaction is formed between the sulfate ion and one of the metal-binding residues, Asn-148. A water molecule also bridges both metals.

TABLE 1

X-ray data collection and structure refinement statistics

Values in parentheses refer to the highest resolution shell. High resolution cutoff was guided by the correlation coefficient $CC_{1/2}$ (35). Zn-SAD, zinc single wavelength anomalous diffraction; CCano, anomalous correlation coefficient; CMCF, Canadian Macromolecular Crystallography Facility; CLS, Canadian Light Source. MacCHESS, Macromolecular Diffraction Facility at the Cornell High Energy Synchrotron Source. r.m.s., root mean square.

Parameters	Sulfate-bound	PC-bound	AMPCP-bound	Sulfate-bound (tetragonal)	Zinc-inhibited	AMP-bound	Crystal used for Zn-SAD
PDB code	5FC1	5FC5	5FC6	5FC7	5FCA	5FCB	
Data collection							
Beamline	08ID-1, CMCF, CLS	F1, MacCHESS	08ID-1, CMCF, CLS	08ID-1, CMCF, CLS	08B1–1, CMCF, CLS	08ID-1, CMCF, CLS	08ID-1, CMCF, CLS
Wavelength (Å)	0.97949	0.91790	0.97949	0.97949	1.28137	0.97949	1.28223
Space group	C 2 2 2_1	C 2 2 2_1	C 2 2 2_1	P 4_1	P 2_1 2_1 2_1	C 2 2 2_1	C 2 2 2_1
Unit cell dimensions (Å)	123.65 131.87 80.06	123.734 132.90 80.14	124.35 132.89 80.52	87.39 87.39 79.84	80.14 123.59 131.61	124.03 132.38 79.74	123.70 132.63 80.36
Unit cell angles (°)	90 90 90	90 90 90	90 90 90	90 90 90	90 90 90	90 90 90	90 90 90
Resolution range (Å)	48.93-1.389 (1.439-1.389)	28.25-1.678 (1.738-1.678)	45.4-1.658 (1.717-1.658)	36.31-1.456 (1.508-1.456)	39.31-1.924 (1.993-1.924)	39.87-1.550 (1.605-1.550)	50.00-1.770 (1.83-1.770)
Resolution at CCano = 30% (Å)					2.88		2.37
Total reflections	1,606,469	952,273	567,906	450,079	2,339,663	582,620	824,926
Unique reflections	124,089 (7898)	68,190 (3859)	78,590 (7430)	100,829 (7376)	93,218 (6018)	89,133 (6001)	63,961 (5816)
Multiplicity	12.9 (2.8)	14.0 (11.5)	7.2 (5.6)	4.5 (1.9)	25.1 (6.7)	6.5 (2.6)	12.9 (5.6)
Completeness (%)	94.7 (61.9)	90.4 (52.8)	99.6 (97.4)	96.4 (72.2)	93.6 (61.7)	93.7 (63.8)	99.0 (91.2)
$I/\sigma(I)$	23.5 (0.5)	17.1 (0.4)	15.8 (0.8)	15.0 (0.3)	23.8 (0.5)	19.7 (0.6)	15.7 (1.0)
Wilson B-factor (Å^2)	20.24	29.44	22.78	25.35	37.92	23.5	
R_{meas} (%)	9.4 (>100)	12.2 (>100)	10.6 (>100)	7.4 (>100)	11.9 (>100)	8.6 (>100)	13.4 (>100)
$CC_{1/2}$ (%)	(15)	(17)	(24)	(16)	(39)	(20)	(17)
Refinement							
Reflections used in refinement	123,471 (7329)	66,735 (3350)	78,503 (7350)	98,417 (5318)	92,449 (5359)	88,924 (5829)	
Reflections used for R-free	6150 (348)	3355 (176)	3932 (377)	1957 (114)	1983 (112)	4411 (264)	
R-work	0.1293 (0.4420)	0.1734 (0.3815)	0.1622 (0.3534)	0.1539 (0.4304)	0.1754 (0.3889)	0.1592 (0.3815)	
R-free	0.1609 (0.4896)	0.2034 (0.3868)	0.1913 (0.3923)	0.1827 (0.4473)	0.2034 (0.4227)	0.1871 (0.4004)	
Number of non-hydrogen atoms	4298	4165	4208	3979	8138	4198	
Macromolecules	3485	3457	3470	3401	6904	3463	
Ligands	268	220	218	172	426	223	
Solvent	545	488	520	406	808	512	
Protein residues	426	426	426	423	852	426	
r.m.s. (bonds) (Å)	0.02	0.005	0.01	0.009	0.012	0.007	
r.m.s. (angles) (°)	1.66	0.98	1.15	1.09	1.23	1.05	
Ramachandran favored (%)	96	96	96	96	96	96	
Ramachandran allowed (%)	4.3	4.3	4.1	3.7	4.2	4.1	
Ramachandran outliers (%)	0	0	0	0	0	0	
Rotamer outliers (%)	0.5	0.51	0.51	0.52	0.77	0.51	
Clashscore	4.02	1.92	1.37	2.7	2.75	1.51	
Average B-factor (Å^2)	30.33	40.26	31.32	33.88	48.38	33.06	
Macromolecules	25.54	36.72	27.44	31.35	45.27	29.13	
Ligands	69.11	80.77	71.9	66.63	94.13	70.67	
Solvent	41.91	47.1	40.17	41.21	50.87	43.22	

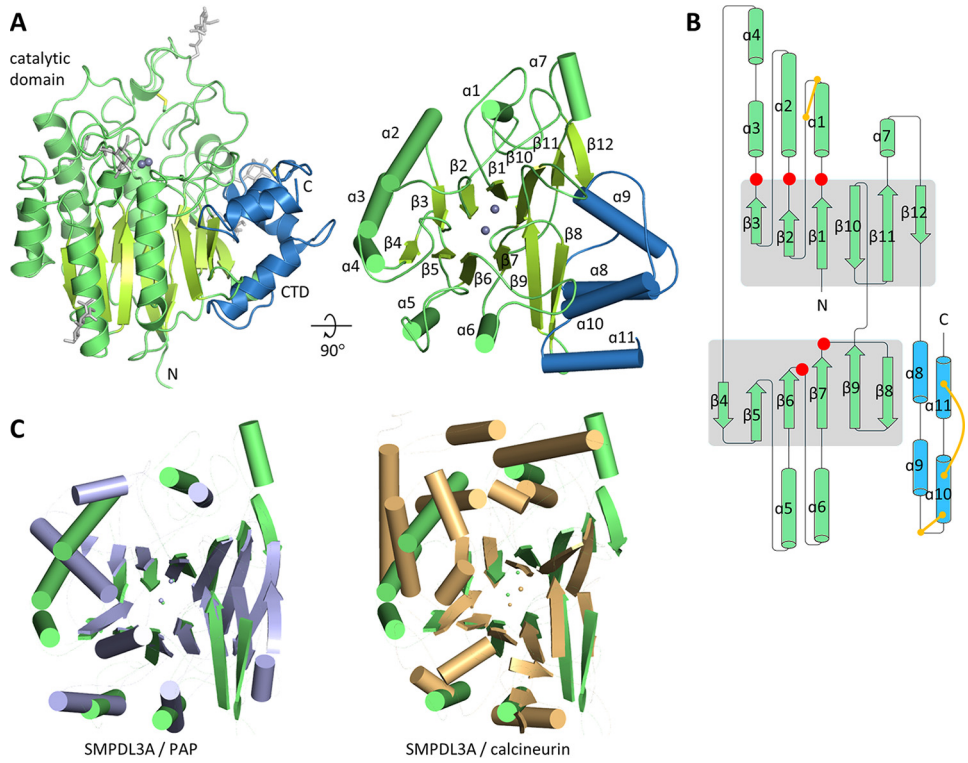

FIGURE 2. **Structure of SMPDL3A.** *A*, the core catalytic domain is shown in *green*, and the CTD is in *blue*. Disulfide bonds appear as *yellow sticks*. *N*-Linked glycans (*white sticks*) are only partially displayed for clarity. The two zinc ions in the active site are represented by *spheres*. N and C termini as well as secondary structure elements are labeled. *B*, topology diagram of SMPDL3A. The central β-sheets are shown in *gray rectangles*. Disulfide bonds are represented by *yellow connectors*. *Red circles* indicate locations of metal binding or catalytic residues. *C*, the β-sandwich fold of SMPDL3A (*green*) is comparable with that of related phosphoesterases including the purple acid phosphatase (*PAP*, PDB code 1WAR, overall sequence identity = 11%, root mean square deviation = 1.5 Å for 46 corresponding α-carbons from the conserved β-strands only), shown in *violet*, and calcineurin (PDB code 3LL8, overall sequence identity = 11%, root mean square deviation = 2.6 Å for 46 corresponding α-carbons from the conserved β-strands only) displayed in *gold*. The loop regions and the CTD of SMPDL3A are hidden for clarity.

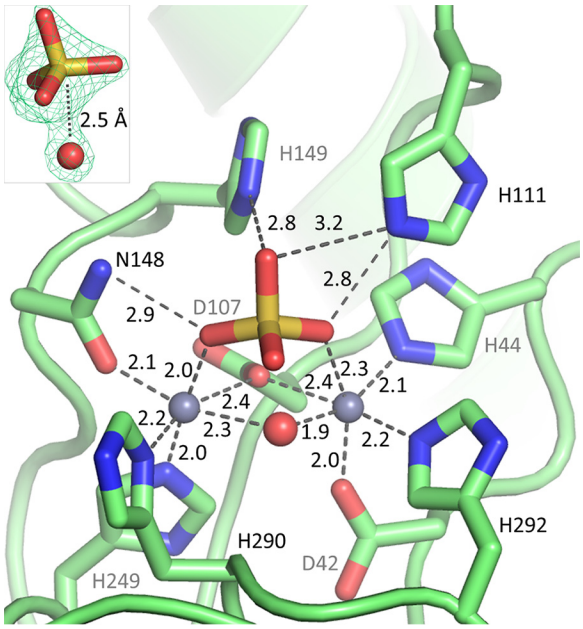

FIGURE 3. **Active site of SMPDL3A.** Residues that coordinate the two zinc ions (*gray spheres*) are shown as sticks, as are the two histidines (His-111 and His-149) interacting with a sulfate ion (*sticks*). The electron density for the water molecule (*red sphere*) located midway between the zinc ions and for the sulfate ion is displayed as a $F_o - F_c$-simulated annealing omit map contoured at 8σ. Distances are indicated (Å).

SMPDL3A is part of a superfamily of phosphoesterases that utilize two metal cations for catalysis. Although ASMase is known to require zinc for activity (5), SMPDL3A was shown to be inhibited by zinc (11). As all metal-coordinating residues are conserved between both proteins (Fig. 1), this finding was rather perplexing. Thus, we sought to further investigate the cation dependence of SMPDL3A. When purified from insect cell media, the recombinant enzyme is catalytically active, and x-ray absorption scans on the protein crystals indicated the presence of zinc (data not shown). We found that low concentrations of zinc ranging from 5 to 100 μM caused the hydrolysis rate of the generic phosphodiesterase substrate bis(*p*-nitrophenyl) phosphate by SMPDL3A to double (data not shown). However, increasingly higher concentrations of zinc did indeed inhibit the enzyme as reported (11), most noticeably at neutral pH. To understand the structural basis for this inhibition, we determined the structure SMPDL3A in the presence of supraphysiological levels of zinc (10 mM). Under these conditions we found that a third zinc ion becomes bound by the protein, coordinated by the side chains of His-149 and His-111 (Fig. 4). The third zinc actually blocks the active site by occupying the location where the sulfate or substrate phosphate group binds under normal conditions. This inhibition could be reversed by mild EDTA treatment to remove the loosely bound third zinc ion. These results suggest that, like ASMase, SMPDL3A is a zinc-dependent enzyme.

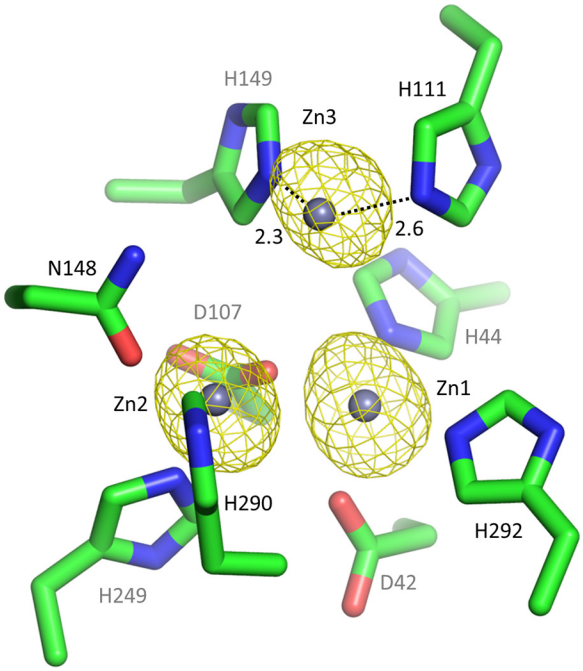

FIGURE 4. **Inhibition of SMPDL3A by excess zinc.** The structure of the protein exposed to a high zinc concentration reveals a third zinc ion bound to the active site. Zinc ions (*spheres*) with their corresponding anomalous difference electron density map peaks (*yellow mesh*) are shown contoured at 10σ.

Substrate Recognition—A variety of substrate specificities exists within the calcineurin-like phosphoesterase superfamily (Pfam code PF00149), including nucleic acids and phosphoproteins. However, as SMPDL3A is most similar to the well studied sphingomyelinase ASMase, the finding that the former hydrolyzes nucleotides rather than lipids (11) was unexpected. To address why SMPDL3A can hydrolyze nucleotides but not SM, we determined its structure in the presence of several possible substrates and reaction products (Fig. 5). It should be noted that the crystallization solution contained 200 mM sulfate, a competitor for the active site, and therefore, substrates may not be present at full occupancy in the crystals. The substrate binding site is a large water-filled T-shaped cavity that emanates from the zinc ions. The crystallization of phosphocholine (*PC*), a product of SM hydrolysis, with SMPDL3A revealed that it can bind to the active site (Fig. 5, *A* and *B*), but the interaction was mediated mainly by the phosphate group. The positively charged choline moiety does not form any specific interactions with the protein that could stabilize it, such as cation-π (29) or electrostatic contacts with negatively charged residues. By contrast, the structure of SMPDL3A bound to AMP shows that in addition to specific phosphate interactions, the adenine ring is positioned in a cleft between the side chains of Gln-324 and Tyr-257 (Fig. 5*C*). This arrangement allows for π stacking between the tyrosine and the adenine base. However, the ribose group of AMP did not stably interact with the protein, and its electron density is fragmented, suggesting conformational flexibility in this region (Fig. 5*D*).

We also crystallized the protein in the presence of the ATP analog AMPCPP, which is uncleavable between the α and β phosphates. However, the electron density map revealed only the presence of AMPCP in the active site, indicating that the γ-phosphate was hydrolyzed by the protein (Fig. 5*E*). The position of the adenine ring of AMPCP is similar to that of AMP, and the electron density map around it is more clearly defined in this case (Fig. 5*F*). One notable difference between the two is the orientation of their terminal phosphate; in AMPCP, the three oxygen atoms coordinate the zinc ions, whereas in AMP, one oxygen points away from them (discussed further below). The terminal phosphate group of both ligands forms hydrogen bonds with His-111, Asn-148, and His-149, although in slightly different manners due to its shift in position. Again, there are no specific interactions between the ribose moiety and the protein.

To assess the importance of the tyrosine involved in stacking interactions with the nucleotide base, kinetic parameters of the wild-type protein were compared with those of the Y257A mutant (Table 2). Activity was assayed at pH 7.5 and 5, reflecting the localization of SMPDL3A in the extracellular space as well as in lysosomes. First, we measured the K_m values for ATP hydrolysis by the wild-type human and murine enzymes at neutral and acidic pH to be in the range of 0.1–1 mM. Affinity for ATP is three to four times higher at acidic pH for both murine and human proteins, possibly due to electrostatic attraction between the negatively charged phosphate groups and protonated histidines His-111 and His-149. Surprisingly, we found that mutation of Tyr-257 in murine SMPDL3A did not affect the K_m for ATP and lowered the turnover number only slightly. These results suggest that Tyr-257 does not contribute significantly to the binding affinity of SMPDL3A for nucleotide substrates. Instead, the cleft formed by Gln-324 and Tyr-257 may simply provide shape complementarity to the base moiety to allow entry of nucleotide substrates while excluding other types of phosphodiester-containing molecules. In this manner SMPDL3A would be able to accommodate a variety of different nucleotide substrates by forming relatively weak nonspecific interactions with their non-phosphate portions, with strong binding affinity arising mainly from contacts between their phosphate groups and His-111, Asn-148, and His-149 as well as the zinc ions.

Proposed Catalytic Mechanism—Comparison of the high resolution structures of SMPDL3A with those of other phosphoesterases from the calcineurin-like superfamily allowed us to propose a nucleotide hydrolysis mechanism for it. An overlay of the active sites of SMPDL3A and calcineurin (30) is shown in Fig. 6*A*. The majority of the metal-coordinating residues are conserved, with the exception of His-292, which is unique to SMPDL3A. Calcineurin is a Ser/Thr phosphatase, and its mechanism of protein dephosphorylation involves a nucleophilic attack by a metal-activated water on the phosphate (28). Importantly, the serine or threonine leaving group is protonated by a histidine residue paired with an aspartate, both highly conserved in the phosphoesterase superfamily (31). In SMPDL3A, His-149 is the corresponding histidine and forms a hydrogen bond to the phosphate (or sulfate) group (Fig. 6*A*). However, the matching aspartate is missing, and instead, an adjacent His-111–Asp-79 pair is present, which also hydrogen-bonds to the phosphate group (Fig. 6*A*). Interestingly, this second histidine is replaced by arginine in calcineurin and suggests that the identity of the histidine protonating the leaving group could be different in SMPDL3A. To determine which histidine

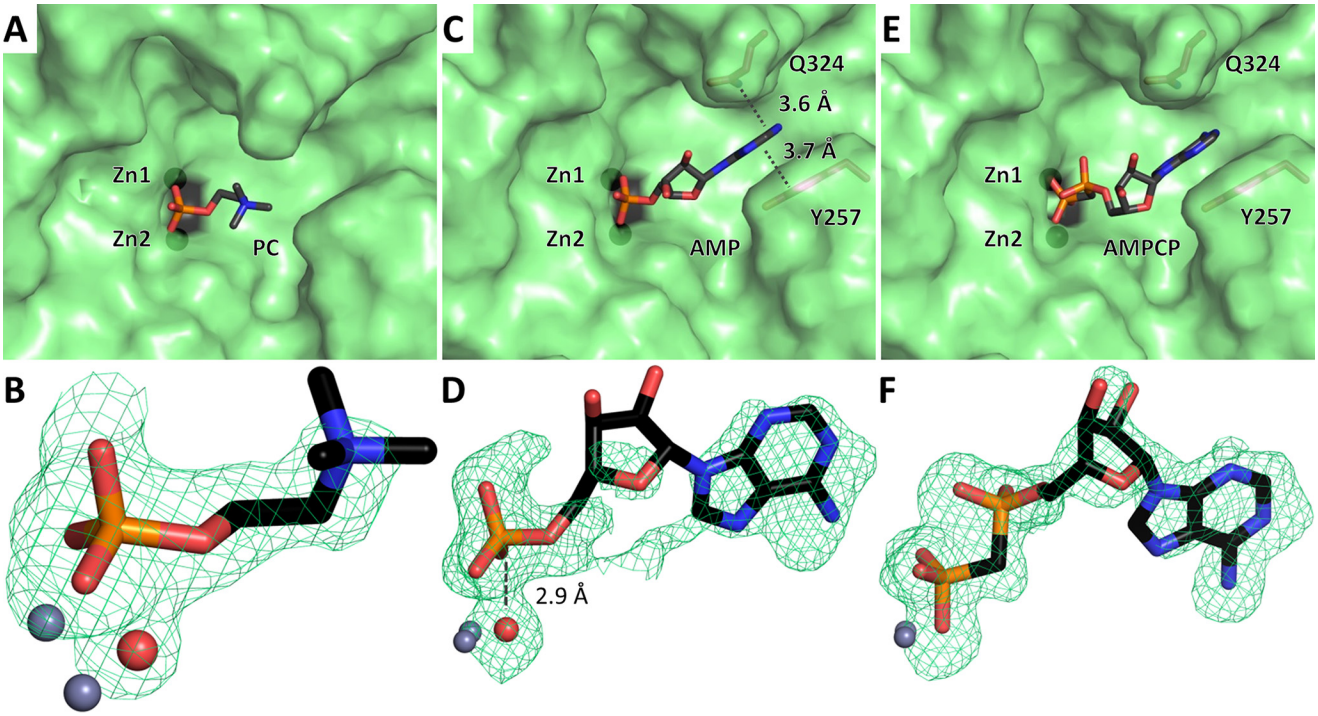

FIGURE 5. **Ligands bound in the active site of SMPDL3A.** The structures of ligands present in the active site are displayed along with their corresponding electron density $F_o - F_c$ simulated annealing omit maps contoured at 3σ. *A* and *B*, phosphocholine (*PC*). *C* and *D*, AMP. *E* and *F*, ADP analog (AMPCP). Zinc ions and water molecules are represented by *gray* and *red spheres*, respectively. The two residues interacting with the adenine base are shown as *sticks* and labeled.

TABLE 2

Michaelis-Menten parameters of ATP hydrolysis by SMPDL3A

Activity of wild-type proteins as well as murine mutants against ATP was assayed. Values are the mean and S.D. of a representative of two experiments performed in triplicates.

Protein	pH 5		pH 7.5	
	k_m	k_{cat}	k_m	k_{cat}
	μM	min^{-1}	μM	min^{-1}
Human WT	174 ± 11	3258 ± 160.3	735 ± 14	168 ± 4.2
Murine WT	107 ± 9	1542 ± 63.6	330 ± 10	260 ± 3.8
Murine Y257A	99 ± 2	860 ± 8.9	310 ± 26	172 ± 6.7
Murine H149Q	466 ± 49	11 ± 0.2	2468 ± 285	2 ± 0.1
Murine H149A	1099 ± 96	1 ± 0.0	–[a]	
Murine H111Q	1163 ± 107	1 ± 0.1	–[a]	
Murine H111A	1221 ± 141	3 ± 0.3	–[a]	

[a] Rates too low for parameter determination.

is responsible for leaving group protonation, kinetic parameters of ATP hydrolysis by the corresponding glutamine or alanine mutants were determined. Mutation of either His-149 or His-111 led to a roughly 10-fold decrease in substrate affinity and lowered the turnover rate by at least 2 orders of magnitude (Table 2). We can, therefore, only conclude that both histidines are essential for the catalytic activity of SMPDL3A, with His-111 assisted by Asp-79 most likely responsible for leaving group protonation.

In calcineurin, the attacking water molecule is located midway between the zinc ions, which are thought to increase its nucleophilicity as well as the electrophilicity of the phosphate moiety (36). An analogous water molecule is visible in the active site of SMPDL3A bound to sulfate, phosphocholine, or AMP (Figs. 3 and 5, *B* and *D*). For the hydrolysis of nucleoside triphosphate substrates into nucleoside diphosphates, the scissile bond is between the γ-phosphorus atom and the oxygen atom bridging it to the β-phosphorus atom (P_γ-O-P_β). This bond cleavage can in theory occur by attack of the nucleophilic water molecule onto either the γ-phosphorus with ADP acting as the leaving group or the β-phosphorus atom with the γ-phosphate as the leaving group. Our structures of SMPDL3A in complex with AMP and AMPCP help us discern between these two possibilities. In the AMP structure, the nucleotide appears to be bound as a *bona fide* substrate with the nucleophilic water molecule poised for attack 2.9 Å away from the AMP phosphorus atom (Figs. 5*D* and 6*B*). Two of the oxygen atoms of the phosphate coordinate the zinc ions, whereas the third oxygen points in the direction opposite the incoming nucleophilic water. However, in the AMPCP structure, the nucleotide appears to be bound as a hydrolysis product of AMPCPP. In this case, the positions of two zinc-coordinating oxygen atoms are essentially the same, but in stark contrast, the orientation of the third oxygen atom is flipped as in an inverted configuration and replaces the position of the attacking water molecule (Fig. 6*B*).

This analysis allowed us to construct a manually docked model of SMPDL3A bound to ATP, the preferred substrates for the enzyme being nucleoside triphosphates (11) (Fig. 6*C*). Importantly, if the γ-phosphate of ATP is placed in the active site, then the ADP leaving group cannot be positioned appropriately to become protonated by His-149/His-111. Only when the β-phosphate is positioned in the active site is the γ-phosphate leaving group hydrogen-bonded by His-149 and His-111 for protonation.

With the β-phosphate of ATP positioned in the active site, the sugar and base moieties are pushed back farther into the cleft between Gln-324 and Tyr-257 than in the case of the

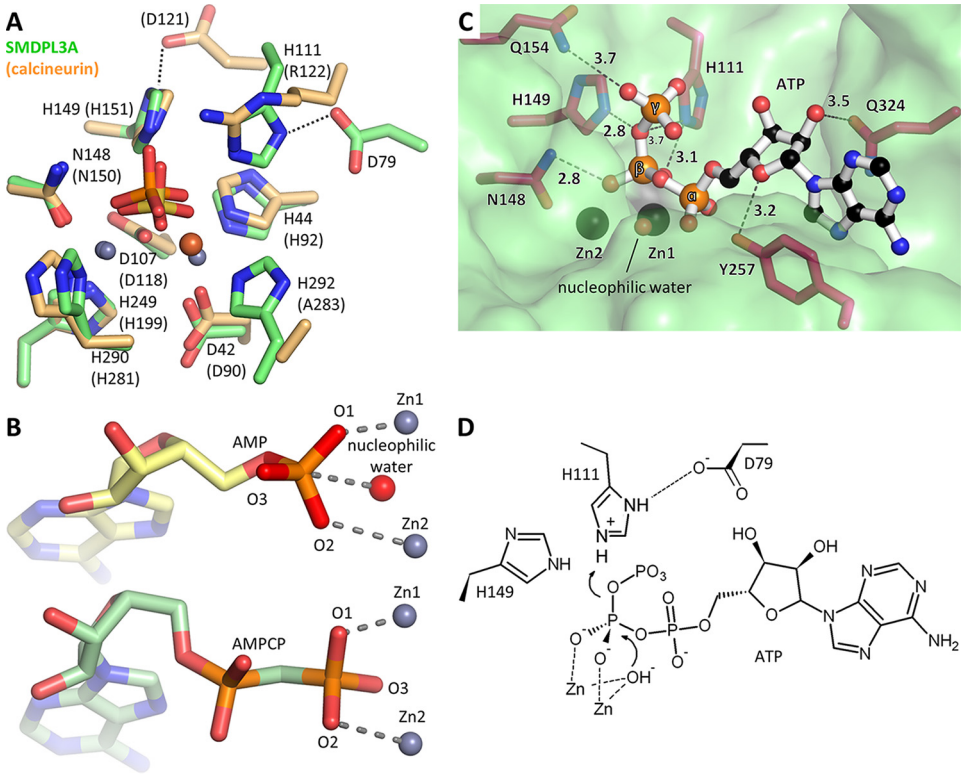

FIGURE 6. **Proposed reaction mechanism for SMPDL3A.** *A*, the active site of SMPDL3A is compared with that of calcineurin (PDB code 3LL8). Residues in beige, one zinc ion, and one iron ion (*orange sphere*) form the calcineurin catalytic center occupied by a phosphate ion (*orange central atom*). Residues in *green* and a sulfate ion (*yellow central atom*) are part of the SMPDL3A active site. Active site residue labels in *parentheses* refer to calcineurin. *B*, a comparison of SMPDL3A bound to AMP and AMPCP is shown (only the ligands are depicted). The structures are in the identical orientation to illustrate the difference in the terminal phosphate group between the two ligands. Zinc ions and the nucleophilic water are labeled. *C*, model of ATP substrate bound to SMPDL3A. An ATP molecule was manually docked into the substrate binding site using the AMP complex structure as a guide. The β-phosphate is positioned for nucleophilic attack by a water molecule (*red sphere*), whereas the γ-phosphate acts as the leaving group. Potential interactions with protein residues are indicated. *D*, schematic diagram of the proposed ATP hydrolysis mechanism for SMPDL3A, which involves a nucleophilic attack by a zinc-activated water molecule on the β-phosphate. This is followed by protonation of the departing γ-phosphate by one of the two nearby histidines, likely His-111 with assistance from Asp-79.

AMP/AMPCP co-crystal structures. This difference could enable hydrogen bonding between the ribose O4′ and Tyr-257 as well as between O_2' and Gln-324, although the wide binding site precluded modeling the orientation of the ribose with great certainty. These additional potential interactions may in part explain the preference for nucleotide triphosphate substrates by SMPDL3A. In this arrangement, the β-phosphate makes contacts with the zinc ions and can undergo nucleophilic attack by the activated water molecule with a concomitant inversion of its configuration (Fig. 6*D*). The γ-phosphate leaving group is protonated by either His-149 or His-111 and departs. Similarly, for the conversion of ADP to AMP, the active site would be occupied by the α-phosphate and the terminal β-phosphate would act as the leaving group.

Discussion

This study reports the first structural characterization of a member of the ASMase-like family of enzymes. The architecture of the catalytic domain is similar to other phosphoesterases, whereas the small CTD is unique to the family. The purpose of the CTD is unknown, but based on its tight association with the catalytic domain, it may simply be an extension of the latter. Mutations in the CTD of ASMase have been shown to inactivate the protein (32), but whether this is due to effects on trafficking, activity, or protein stability is unclear.

Unlike SMPDL3A and SMPDL3B, ASMase contains a saposin domain that facilitates binding to membranes and lipids (5). SMPDL3B, in turn, is attached to the membrane via a glycosylphosphatidylinositol anchor (6). The lack of any obvious membrane-interacting features in the SMPDL3A structure, such as the hydrophobic hairpin of bacterial sphingomyelinases (33), may be related to its evolutionary specificity toward the hydrolysis of nucleotides rather than membrane lipids. It should be noted that a number of lipid-degrading enzymes require the assistance of protein cofactors for access to lipids (5), and we cannot exclude this possibility for SMPDL3A.

Although SMPDL3A can accommodate the choline head group of SM in its active site, binding is mediated mainly by the phosphate moiety. Interestingly, in the case of nucleotide substrates, binding affinity also seems to stem mainly from electrostatic and hydrogen-bond interactions involving the β and possibly γ phosphates (or α and β phosphates in nucleotide diphosphates). Interactions with parts of the nucleotide beyond the phosphates are weak and do not contribute significantly to binding as demonstrated by the Y257A mutant. Indeed, this tyrosine is replaced by a serine residue in human SMPDL3A (Fig. 1), which is also active against nucleotides, further confirming that Tyr-257 is not important for substrate binding. We suggest that the relative lack of specific recognition beyond the

phosphate group is what allows this protein to hydrolyze different types of nucleotide triphosphates and diphosphates (11).

Our work reconciles previous findings of inhibition of SMPDL3A by zinc, with the known dependence of ASMase on this metal. Millimolar concentrations of zinc block the active site of the enzyme, and optimal activity is only possible at lower concentrations in the micromolar range, consistent with the physiological serum levels of zinc (5). Excessive zinc concentrations are known to also inhibit ASMase (34). This artificial inhibition is less pronounced at acidic pH, perhaps due to electrostatic repulsion between the metal ions and the partially protonated coordinating histidine residues.

The catalytic mechanism proposed here is similar to that of other members of the calcineurin-like phosphoesterase superfamily, with the identity of the catalytic histidine as a possible key difference. Our mechanism accounts for the ability of SMPDL3A to hydrolyze ATP and ADP while remaining inactive against AMP (11), as there is no possible leaving group when AMP is bound in the same orientation as the other nucleotides. Additionally, it accounts for the much higher K_{cat} of the enzyme at pH 5, as the catalytic histidine would be a better proton donor in an acidic environment. All of the residues involved in the proposed mechanism are conserved in ASMase (Fig. 1). In addition, disulfide-forming cysteines are conserved, and sequence insertions occur only outside of secondary structure elements, suggesting that ASMase adopts the same overall fold, including the CTD. However, there is no sequence conservation with ASMase in residues that interact with the substrate portions beyond the phosphate group (Fig. 1), which could explain the different substrate specificities of these two proteins. This study, therefore, sheds new light on the function of ASMase-like enzymes.

Author Contributions—A. G., G. S.-F., and B. N. designed the experiments, A. G. and K. I. performed the experiments, A. G. and B. N. analyzed the data, and A. G. and B. N. wrote the article. All authors approved the final version of the manuscript.

Acknowledgments—We thank Dr. Guennadi Kozlov and Dr. Shaun Labiuk for x-ray data collection. We are grateful to Dr. Leonhard X. Heinz for advice. The research described in this paper was performed using beamlines 08ID-1 and 08B1-1 at the Canadian Light Source, which is supported by the Canada Foundation for Innovation, Natural Sciences, and Engineering Research Council of Canada, the University of Saskatchewan, the Government of Saskatchewan, Western Economic Diversification Canada, the National Research Council Canada, and the Canadian Institutes of Health Research.

References

1. Castro B. M., Prieto M., and Silva L. C. (2014) Ceramide: a simple sphingolipid with unique biophysical properties. *Prog. Lipid. Res.* **54,** 53–67
2. Ong W. Y., Herr D. R., Farooqui T., Ling E. A., and Farooqui A. A. (2015) Role of sphingomyelinases in neurological disorders. *Expert Opin. Ther. Targets* **19,** 1725–1742
3. Zimmermann H., Zebisch M., and Sträter N. (2012) Cellular function and molecular structure of ecto-nucleotidases. *Purinergic Signal* **8,** 437–502
4. Airola M. V., and Hannun Y. A. (2013) Sphingolipid metabolism and neutral sphingomyelinases. *Handb. Exp. Pharmacol.* **215,** 57–76
5. Kornhuber J., Rhein C., Müller C. P., and Mühle C. (2015) Secretory sphingomyelinase in health and disease. *Biol. Chem.* **396,** 707–736
6. Heinz, L. X., Baumann, C. L., Köberlin, M. S., Snijder, B., Gawish, R., Shui, G., Sharif, O., Aspalter, I. M., Müller, A. C., Kandasamy, R. K., Breitwieser, F. P., Pichlmair, A., Bruckner, M., Rebsamen, M., Blüml, S., Karonitsch, T., Fauster, A., Colinge, J., Bennett, K. L., Knapp, S., Wenk, M. R., and Superti-Furga, G. (2015) The lipid-modifying enzyme SMPDL3B negatively regulates innate immunity. *Cell Rep.* **11,** 1919–1928
7. Masuishi Y., Nomura A., Okayama A., Kimura Y., Arakawa N., and Hirano H. (2013) Mass spectrometric identification of glycosylphosphatidylinositol-anchored peptides. *J. Proteome Res.* **12,** 4617–4626
8. Czupalla C., Mansukoski H., Riedl T., Thiel D., Krause E., and Hoflack B. (2006) Proteomic analysis of lysosomal acid hydrolases secreted by osteoclasts: implications for lytic enzyme transport and bone metabolism. *Mol. Cell. Proteomics* **5,** 134–143
9. Lim J. M., Sherling D., Teo C. F., Hausman D. B., Lin D., and Wells L. (2008) Defining the regulated secreted proteome of rodent adipocytes upon the induction of insulin resistance. *J. Proteome Res.* **7,** 1251–1263
10. Greco T. M., Seeholzer S. H., Mak A., Spruce L., and Ischiropoulos H. (2010) Quantitative mass spectrometry-based proteomics reveals the dynamic range of primary mouse astrocyte protein secretion. *J. Proteome Res.* **9,** 2764–2774
11. Traini M., Quinn C. M., Sandoval C., Johansson E., Schroder K., Kockx M., Meikle P. J., Jessup W., and Kritharides L. (2014) Sphingomyelin phosphodiesterase acid-like 3A (SMPDL3A) is a novel nucleotide phosphodiesterase regulated by cholesterol in human macrophages. *J. Biol. Chem.* **289,** 32895–32913
12. Pehkonen P., Welter-Stahl L., Diwo J., Ryynänen J., Wienecke-Baldacchino A., Heikkinen S., Treuter E., Steffensen K. R., and Carlberg C. (2012) Genome-wide landscape of liver X receptor chromatin binding and gene regulation in human macrophages. *BMC Genomics* **13,** 50
13. Noto P. B., Bukhtiyarov Y., Shi M., McKeever B. M., McGeehan G. M., and Lala D. S. (2012) Regulation of sphingomyelin phosphodiesterase acid-like 3A gene (SMPDL3A) by liver X receptors. *Mol. Pharmacol.* **82,** 719–727
14. Zhou, M., Lucas, D. A., Chan, K. C., Issaq, H. J., Petricoin, E. F., 3rd., Liotta, L. A., Veenstra, T. D., and Conrads, T. P. (2004) An investigation into the human serum "interactome." *Electrophoresis* **25,** 1289–1298
15. Veenstra T. D., Conrads T. P., Hood B. L., Avellino A. M., Ellenbogen R. G., and Morrison R. S. (2005) Biomarkers: mining the biofluid proteome. *Mol. Cell. Proteomics* **4,** 409–418
16. Padilla, J., Jenkins, N. T., Lee, S., Zhang, H., Cui, J., Zuidema, M. Y., Zhang, C., Hill, M. A., Perfield, J. W., 2nd., Ibdah, J. A., Booth, F. W., Davis, J. W., Laughlin, M. H., and Rector, R. S. (2013) Vascular transcriptional alterations produced by juvenile obesity in Ossabaw swine. *Physiol. Genomics* **45,** 434–446
17. Perisic, L., Hedin, E., Razuvaev, A., Lengquist, M., Osterholm, C., Folkersen, L., Gillgren, P., Paulsson-Berne, G., Ponten, F., Odeberg, J., and Hedin, U. (2013) Profiling of atherosclerotic lesions by gene and tissue microarrays reveals PCSK6 as a novel protease in unstable carotid atherosclerosis. *Arterioscler. Thromb. Vasc. Biol.* **33,** 2432–2443
18. Sawada, H., Takami, K., and Asahi, S. (2005) A toxicogenomic approach to drug-induced phospholipidosis: analysis of its induction mechanism and establishment of a novel *in vitro* screening system. *Toxicol. Sci.* **83,** 282–292
19. Anthérieu, S., Rogue, A., Fromenty, B., Guillouzo, A., and Robin, M. A. (2011) Induction of vesicular steatosis by amiodarone and tetracycline is associated with up-regulation of lipogenic genes in HepaRG cells. *Hepatology* **53,** 1895–1905
20. Sleat, D. E., Jadot, M., and Lobel, P. (2007) Lysosomal proteomics and disease. *Proteomics Clin. Appl.* **1,** 1134–1146
21. Qian, M., Sleat, D. E., Zheng, H., Moore, D., and Lobel, P. (2008) Proteomics analysis of serum from mutant mice reveals lysosomal proteins selectively transported by each of the two mannose 6-phosphate receptors. *Mol. Cell. Proteomics* **7,** 58–70
22. Sleat, D. E., Wiseman, J. A., Sohar, I., El-Banna, M., Zheng, H., Moore, D. F., and Lobel, P. (2012) Proteomic analysis of mouse models of Niemann-Pick C disease reveals alterations in the steady-state levels of lysosomal proteins within the brain. *Proteomics* **12,** 3499–3509
23. Airola, M. V., Tumolo, J. M., Snider, J., and Hannun, Y. A. (2014) Identification and biochemical characterization of an acid sphingomyelinase-

like protein from the bacterial plant pathogen Ralstonia solanacearum that hydrolyzes ATP to AMP but not sphingomyelin to ceramide. *PLoS ONE* **9,** e105830
24. Berger, I., Fitzgerald, D. J., and Richmond, T. J. (2004) Baculovirus expression system for heterologous multiprotein complexes. *Nat. Biotechnol.* **22,** 1583–1587
25. Otwinowski, Z., and Minor, W. (1997) Processing of x-ray diffraction data collected in oscillation mode. *Methods Enzymol.* **276,** 307–326
26. Adams, P. D., Afonine, P. V., Bunkóczi, G., Chen, V. B., Davis, I. W., Echols, N., Headd, J. J., Hung, L. W., Kapral, G. J., Grosse-Kunstleve, R. W., McCoy, A. J., Moriarty, N. W., Oeffner, R., Read, R. J., Richardson, D. C., Richardson, J. S., Terwilliger, T. C., and Zwart, P. H. (2010) PHENIX: a comprehensive Python-based system for macromolecular structure solution. *Acta Crystallogr. D Biol. Crystallogr.* **66,** 213–221
27. Emsley, P., and Cowtan, K. (2004) Coot: model-building tools for molecular graphics. *Acta Crystallogr. D Biol. Crystallogr.* **60,** 2126–2132
28. Shi, Y. (2009) Serine/threonine phosphatases: mechanism through structure. *Cell* **139,** 468–484
29. Cheng, J., Goldstein, R., Gershenson, A., Stec, B., and Roberts, M. F. (2013) The cation-π box is a specific phosphatidylcholine membrane targeting motif. *J. Biol. Chem.* **288,** 14863–14873
30. Li, H., Pink, M. D., Murphy, J. G., Stein, A., Dell'Acqua, M. L., and Hogan, P. G. (2012) Balanced interactions of calcineurin with AKAP79 regulate Ca^{2+}-calcineurin-NFAT signaling. *Nat. Struct. Mol. Biol.* **19,** 337–345
31. Rusnak, F., and Mertz, P. (2000) Calcineurin: form and function. *Physiol. Rev.* **80,** 1483–1521
32. Zampieri, S., Filocamo, M., Pianta, A., Lualdi, S., Gort, L., Coll, M. J., Sinnott, R., Geberhiwot, T., Bembi, B., and Dardis, A. (2016) SMPD1 mutation update: database and comprehensive analysis of published and novel variants. *Hum. Mutat.* **37,** 139–147
33. Ago, H., Oda, M., Takahashi, M., Tsuge, H., Ochi, S., Katunuma, N., Miyano, M., and Sakurai, J. (2006) Structural basis of the sphingomyelin phosphodiesterase activity in neutral sphingomyelinase from *Bacillus cereus*. *J. Biol. Chem.* **281,** 16157–16167
34. Schissel, S. L., Keesler, G. A., Schuchman, E. H., Williams, K. J., and Tabas, I. (1998) The cellular trafficking and zinc dependence of secretory and lysosomal sphingomyelinase, two products of the acid sphingomyelinase gene. *J. Biol. Chem.* **273,** 18250–18259
35. Karplus, P. A., and Diederichs, K. (2012) Linking crystallographic model and data quality. *Science* **336,** 1030–1033
36. Andreini, C., Bertini, I., Cavallaro, G., Holliday, G. L., and Thornton, J. M. (2008) Metal ions in biological catalysis: from enzyme databases to general principles. *J. Biol. Inorg. Chem.* **13,** 1205–1218